Application of the Modified Page-Hinkley Test to Diagnose Current Sensor Faults in Induction Motor Drives

Cuong Dinh Tran
Power System Optimization Research Group, Faculty of Electrical and Electronics Engineering, Ton Duc Thang University, Ho Chi Minh City, Vietnam
trandinhcuong@tdtu.edu.vn (corresponding author)

Martin Kuchar
Department of Applied Electronics, Faculty of Electrical Engineering and Computer Science, VSB-Technical University of Ostrava, Ostrava, Czechia
martin.kuchar@vsb.cz

Phuong Duy Nguyen
Department of Applied Electronics, Faculty of Electrical Engineering and Computer Science, VSB-Technical University of Ostrava, Ostrava, Czechia | Faculty of Engineering and Technology, Saigon University, Ho Chi Minh City, Vietnam
phuong.nguyen.duy.st@vsb.cz

Received: 23 August 2025 | Revised: 4 October 2025 and 22 October 2025 | Accepted: 1 November 2025

 DOI: https://doi.org/10.48084/etasr.14256

ABSTRACT

This paper investigates improving reliability in Induction Motor (IM) drives using the Field-Oriented Control (FOC) technique by developing a Modified Page–Hinkley Test (MPHT) for real-time detection of Current Sensor Faults (CSFs). The proposed method monitors the absolute residual between the measured stator current and the corresponding estimated obtained value from a Luenberger Observer (LO). The modified test is implemented in a stepwise manner to ensure high sensitivity to faults and robustness against measurement noise. Upon fault detection, the observer seamlessly reconstructs the faulty current signal to maintain stable closed-loop operation without re-tuning the controller. Simulation studies performed in MATLAB/Simulink under various types of soft (drift, scale, offset, precision degradation), and hard (constant value, constant with noise) faults confirm fast fault detection, accurate fault isolation, and stable system performance. The results show that the proposed method provides a practical and efficient solution for IM drive systems under dynamic operating conditions.

Keywords-induction motor drive; field-oriented control; current sensor fault detection; Luenberger observer; Page–Hinkley test

I. INTRODUCTION

IMs have long been the preferred choice in a wide variety of applications, from industrial automation to electric transportation [1], due to their simple structure and high durability. Regarding control techniques, FOC is a popular approach to achieve precise regulation of both torque and flux [2, 3]. Advances have expanded the scope of FOC, including its application to electric vehicles [4, 5], its extension to polyphase machines via advanced converter topologies [6], and the development of current sensorless strategies, such as virtual current methods [7] and Model Reference Adaptive System (MRAS) based estimators [8]. These contributions confirm the central role of FOC in IM drives, which typically integrate four main subsystems: motor, voltage source inverter, controller, and sensor system.

Despite its multiple advantages, FOC relies on accurate current measurements, making the drive highly susceptible to sensor faults. In particular, CSFs can lead to severe performance degradation or even instability, highlighting the need for Fault-Tolerant Control (FTC). The latter has been extensively studied to improve the reliability of IM drives under sensor failure conditions. Nevertheless, existing approaches, including sensorless strategies [9], observer-based methods [10, 11], and current space vector techniques [12], remain computationally demanding and sensitive to parameter variations. Some also show limited accuracy under noisy

environments [13]. Counter-based fault detection mechanisms, where faults are recognized after a number of consecutive threshold crossings of the current or speed signal, have been proposed [14, 15]. Although this method is simple and easy to implement, it causes a significant delay in fault detection (typically requiring 20–35 sampling cycles, equivalent to 2–3.5 ms at 10 kHz) and may miss transient faults in noisy environments. In [16], an Artificial Neural Network (ANN)-based fault detector was trained to recognize CSFs in a vector control system. The simulation results show that the optimal ANN configuration achieves a detection time (Δt) of Δt_{det} = 0.22 ms, along with the smallest Integral of Square of the Error (ITSE) and Integral Time Absolute Error (ITAE) values among the compared models. However, as the detection delay increases, both the ITSE and ITAE indices rise significantly since control errors accumulate over longer periods before the compensation mechanism is activated. Notably, under low-speed operation, the ANN-based detector exhibited an oscillation delay of up to 8.0 ms for the phase-B sensor fault, indicating reduced sensitivity due to the lower signal-to-noise ratio at this condition [16]. This limitation highlights the need for faster fault detection methods that are statistically sound and capable of distinguishing real faults from random fluctuations in real time.

Beyond FTC schemes, signal processing methods have also been investigated for IM Fault Diagnosis (FD). Fourier-based spectral analysis is widely applied due to its simplicity, although it is limited to stationary signals and noise sensitivity [17]. To address these drawbacks, wavelet and time-frequency techniques have been explored for rotor fault detection [18]. Hybrid approaches combining mechanical and electrical signals have also been proposed [19], while Discrete Wavelet Transform (DWT) integrated with ANNs has achieved high diagnostic accuracy in distinguishing incipient faults [20]. Despite these advances, current methods remain inadequate.

Building on previous Page Hinkley-based change detection techniques [21, 22], this study introduces the MPHT integrated with an LO [23, 24] to enhance CSF detection and fault compensation in IM drives. The residual value between the measured and estimated currents serves as the detection input, allowing the MPHT to distinguish real sensor faults from random noise. When a fault is detected, the faulty current measurement is seamlessly replaced by the observer's estimated signal, ensuring uninterrupted FOC. Fault simulation experiments validate the effectiveness of the proposed scheme, demonstrating rapid detection, low false alarm rate, and improved operational sustainability of the IM drive.

II. MATHEMATICAL MODEL OF INDUCTION MOTOR

A. Mathematical Model in the (α, β) Stationary Reference Frame

The relationship between current, voltage, and flux in an IM can be expressed through a system of first-order differential equations [25]. In the static reference frame (α, β), the stator current vector and rotor flux components corresponding to the input voltage and motor parameters are governed by:

$$\frac{di_{s\alpha}}{dt} = -K_1 i_{s\alpha} + K_2 \psi_{r\alpha} + K_3 \omega_r \psi_{r\beta} + K_4 u_{s\alpha} \quad (1)$$

$$\frac{di_{s\beta}}{dt} = -K_1 i_{s\beta} + K_2 \psi_{r\beta} - K_3 \omega_r \psi_{r\alpha} + K_4 u_{s\beta} \quad (2)$$

$$\frac{d\psi_{r\alpha}}{dt} = K_5 i_{s\alpha} - K_6 \psi_{r\alpha} - \omega_r \psi_{r\beta} \quad (3)$$

$$\frac{d\psi_{r\beta}}{dt} = K_5 i_{s\beta} - K_6 \psi_{r\beta} - \omega_r \psi_{r\alpha} \quad (4)$$

where $u_{s\alpha}, u_{s\beta}$ are the stator voltage components, $i_{s\alpha}, i_{s\beta}$ are the stator current vector, $\psi_{r\alpha}, \psi_{r\beta}$ are the rotor flux linkage components, ω_r is the rotor speed, R_s, R_r are the stator and rotor resistances, L_s, L_r, L_m are the stator, rotor, and magnetizing inductances, and K_i are constants.

$$K_1 = \frac{R_s L_r^2 + R_r L_m^2}{L_s L_r^2 \sigma};\ K_2 = \frac{R_r L_m}{L_s L_r^2 \sigma};\ K_3 = \frac{L_m}{L_s L_r \sigma};$$

$$K_4 = \frac{1}{L_s \sigma};\ K_5 = \frac{R_r L_m}{L_r};\ K_6 = \frac{R_r}{L_r};\ \text{with } \sigma = \frac{L_s L_r - L_m^2}{L_s L_r}$$

B. Field-Oriented Control

The FOC strategy enables decoupled control of flux and torque in an IM by transforming the three-phase stator currents (i_a, i_b, i_c) into the stationary orthogonal reference frame (α, β) using the Clarke transformation. Subsequently, the (α, β) components are transformed into the rotating reference frame (x, y), in which the x-axis is aligned with the rotor flux vector, using the Park transformation [26]. These steps are expressed mathematically as:

$$\begin{cases} i_{s\alpha} = i_a \\ i_{s\beta} = \frac{1}{\sqrt{3}} i_a + \frac{2}{\sqrt{3}} i_b \end{cases} \quad (5)$$

$$\begin{cases} i_{sx} = i_{s\alpha} \cos\gamma + i_{s\beta} \sin\gamma \\ i_{sy} = -i_{s\alpha} \sin\gamma + i_{s\beta} \cos\gamma \end{cases} \quad (6)$$

where γ is the instantaneous position of the rotating reference frame, which is typically aligned with the rotor flux vector. Here, i_{sx} is the direct-axis current component responsible for regulating the rotor flux magnitude, while i_{sy} is the quadrature-axis current component controlling the electromagnetic torque.

The FOC scheme typically employs a cascade control architecture consisting of an outer speed control loop and inner current control loops, which are implemented using Proportional-Integral (PI) controllers to achieve independent regulation of torque and flux. Based on the reference rotor speed ω_r^* and reference rotor flux ψ_r^*, the FOC algorithm computes the required voltage commands for the voltage source inverter. The complete configuration of the FOC system is shown in Figure 1.

The rotor flux vector ψ_r is estimated in real time using a flux observer, while the actual rotor speed ω_r is measured through an incremental encoder for closed-loop feedback. This control structure ensures accurate torque production, rapid transient response, and robustness under varying load conditions. Compared to typical scalar control methods, FOC provides higher precision, improved dynamic performance, and superior adaptability for high-performance drive applications.

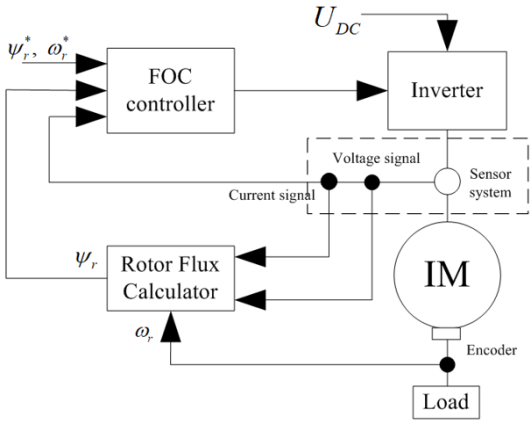

Fig. 1. Block diagram of the FOC structure [3].

III. CURRENT SENSOR FAULT MODELING

A. Fault Classification

SFs in current measurement can be classified into two main types: soft faults (including offset, drift, scale, and precision degradation) and hard faults (including constant signal, constant value with noise, or bottom noise). These faults can significantly reduce the performance and stability of FOC-based motor drives. To accurately model the fault signals, mathematical expressions for each type of fault are used and defined in Table I. The standard deviation of the sensor noise is considered negligible in this analysis.

TABLE I. MATHEMATICAL EXPRESSIONS FOR TYPICAL CURRENT SENSOR FAULT TYPES

Fault type	**Expression for measured signal $i_{meas}(t)$**
Drift	$i_{meas}(t) = i_{true}(t) + a.t$
Scale	$i_{meas}(t) = a.i_{true}(t)$
Bias	$i_{meas}(t) = i_{true}(t) + b$
Precision degradation	$i_{meas}(t) = i_{true}(t) + n(t)$
Constant fault	$i_{meas}(t) = C$
Constant with noise	$i_{meas}(t) = C + n(t)$
Bottom noise	$i_{meas}(t) = n(t)$

where a is the scale factor, b is the shift factor, n is the decomposition level, and C is the wavelet coefficient.

Table I summarizes the mathematical formulations for different fault types. Soft faults such as drift, scale, and bias introduce predictable deviations in the sensor output, whereas hard faults lead to constant or completely erroneous readings. Collectively, these models form the basis for generating faulty signal scenarios used to simulate and test the proposed fault detection algorithm.

B. Integration of Fault Diagnosis in Field-Oriented Control

Under normal operating conditions, the FOC strategy requires accurate measurement of the three-phase stator currents. These are first converted to the stationary two-phase coordinate system (α, β), and then to the co-rotating coordinate system (x, y) to realize the separate control of the magnetic flux and torque. However, in practice, current sensors may encounter problems such as broken circuits, value deviations, or signal drifts, which degrade the control performance or even cause system instability. To overcome this issue, an FD mechanism is integrated into the IM drive.

The FD block detects abnormal sensor behaviors and automatically restructures the control algorithm to maintain stable system operation. The overall control structure integrating the FOC strategy with the FD block is displayed in Figure 2.

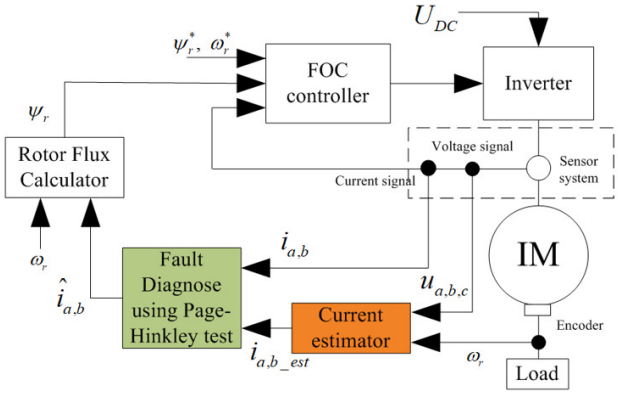

Fig. 2. FOC scheme, including an FD block for the IM drive.

IV. FAULT DIAGNOSIS CONTROL FRAMEWORK

A. Luenberger Observer for Current Estimation

In the system, an LO estimates the stator current space vector components in the (α, β) reference frame, as given by (7-10). Its accuracy relies on the input angular speed. Using the actual rotor speed from an encoder, the LO accurately reflects the IM's behavior:

$$\frac{di_{s\alpha\_est}}{dt} = -K_1 i_{s\alpha\_est} + K_2 \psi_{r\alpha\_est} + K_3 \omega_r \psi_{r\beta\_est} + K_4 u_{s\alpha} - L_1 i_{s\alpha\_est} + L_2 i_{s\beta\_est} \quad (7)$$

$$\frac{di_{s\beta\_est}}{dt} = -K_1 i_{s\beta\_est} - K_3 \omega_r \psi_{r\alpha\_est} + K_2 \psi_{r\beta\_est} + K_4 u_{s\beta} - L_1 i_{s\beta\_est} - L_2 i_{s\alpha\_est} \quad (8)$$

$$\frac{d\psi_{r\alpha\_est}}{dt} = K_5 i_{s\alpha\_est} - K_6 \psi_{r\alpha\_est} - \omega_r \psi_{r\beta\_est} - L_3 i_{s\alpha\_est} + L_4 i_{s\beta\_est} \quad (9)$$

$$\frac{d\psi_{r\beta\_est}}{dt} = K_5 i_{s\beta\_est} + \omega_r \psi_{r\alpha\_est} - K_6 \psi_{r\beta\_est} + L_3 i_{s\beta\_est} - L_4 i_{s\alpha\_est} \quad (10)$$

where:

$$L_1 = (k-1)\left(\frac{1}{\sigma T_s} + \frac{1}{\sigma T_r}\right);\ L_2 = -(k-1)\omega_r;$$

$$L_3 = (k^2-1)\left[\left(\frac{1}{\sigma T_s} + \frac{1}{\sigma T_r}\right)\frac{\sigma L_s L_m}{L_r} - \frac{L_m}{T_r}\right] + \frac{\sigma L_s L_m}{L_r}\left(\frac{1}{\sigma T_s} + \frac{1}{\sigma T_r}\right)(k-1);$$

$$L_4 = -(k-1)\frac{\sigma L_s L_m}{L_r}\omega_r;\ T_s = \frac{L_s}{R_s};\ T_r = \frac{L_r}{R_r};\ k > 1;$$

To interface the estimated stator current components in the stationary frame with the three-phase domain required for the fault detection and control structure, an inverse Clarke transformation is applied to convert i_α and i_β into phase currents i_a and i_b as described in:

$$\begin{cases} i_{a\_est} = i_{\alpha\_est} \\ i_{b\_est} = -\frac{1}{2} i_{\alpha\_est} + \frac{\sqrt{3}}{2} i_{\beta\_est} \end{cases} \quad (11)$$

B. Modified Page-Hinkley Test for Fault Detection

To detect CSFs in real time, the MPHT is applied to the absolute residual signal, defined as the difference between the measured stator current and the corresponding estimated value obtained from the LO. This equation allows the detection of both positive and negative offsets, ensuring reliability against sensor faults due to drift or phase shift. The absolute residual is computed using:

$$r_{abs}(t) = \left| i_{meas}(t) - i_{est}(t) \right| \quad (12)$$

where $i_{meas}(t)$ is the measured stator current from the sensor and $i_{est}(t)$ is the estimated current from LO.

The PHT statistic S(t) is computed incrementally using:

$$S(t) = S(t-1) + \left[r_{abs}(t) - \delta/2 \right] \quad (13)$$

where δ is a user-defined tolerance for the expected average absolute residual under nominal conditions.

The minimum of S(t) is tracked using:

$$m_S(t) = \min\left[m_S(t-1), S(t) \right] \quad (14)$$

The PHT decision statistic is given by:

$$PH(t) = S(t) - m_S(t) \quad (15)$$

A binary fault flag, defined in (16), is latched if the decision statistic exceeds a predefined threshold:

$$F(t) = \begin{cases} 1, & \text{if } PH(t) > \lambda \\ 0, & \text{otherwise} \end{cases} \quad (16)$$

where λ is the threshold for fault declaration.

Two parameters control the detection sensitivity: the expected absolute residual under normal operation, $\delta = 0.08$, and the detection threshold, $\lambda = 0.4$. An external binary reset signal is used to reset the MPHT memory, including $S(t)$, $m_S(t)$ and the fault latch flag. This allows the system to clear the fault state after fault handling or acknowledgment.

Figure 3 depicts a block diagram of the MPHT algorithm for diagnosing CSFs. The diagram illustrates the process of calculating the absolute residual value, incrementally updating the decision statistics, and triggering the faulty flag (Fa, Fb) when the thresholds are exceeded. The faulty current signal is then replaced by an observer-based estimate, thereby ensuring the reliable operation of the IM drive under sensor fault conditions.

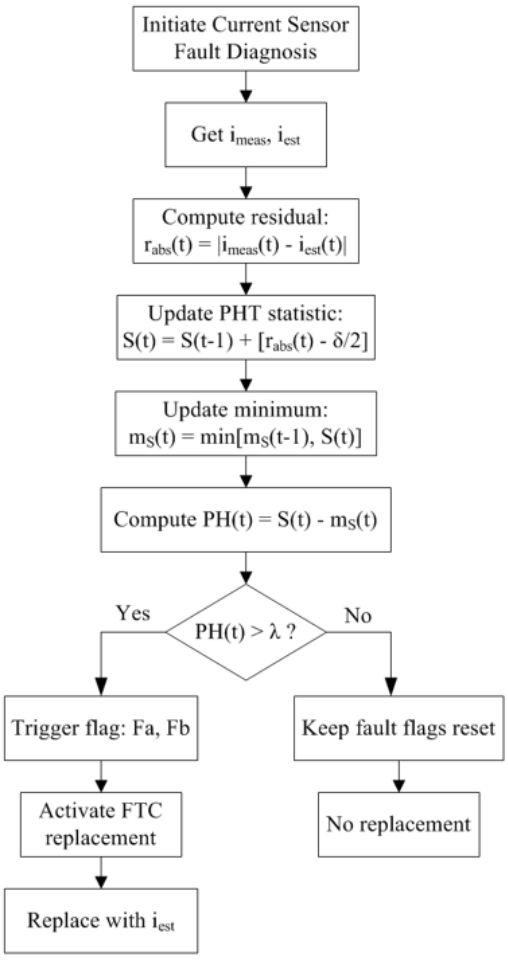

Fig. 3. Flowchart of the MPHT algorithm for current sensor fault FD.

Unlike conventional PHT techniques that rely on signed residuals, the proposed MPHT method uses absolute residuals as the error detection input. This improvement significantly increases the sensitivity to both positive and negative deviations, allowing for fast and reliable error detection. In addition, MPHT continuously evaluates the cumulative average

deviation of the observed residual signal, allowing the algorithm to react to long-lasting deviations in just a few sampling cycles (< 1 ms) without the need for fixed counters or manual threshold adjustments. The statistical formulation of the algorithm also provides strong anti-interference ability and ensures stable and reliable operation under real-time conditions.

The FD module performs three main functions: (i) evaluating the operating status of the current sensor by PH index, (ii) triggering the corresponding fault current sensor flags (Fa, Fb) when anomalies are detected, and (iii) reconfiguring the proper current signal to the FOC controller, as shown in Figure 4.

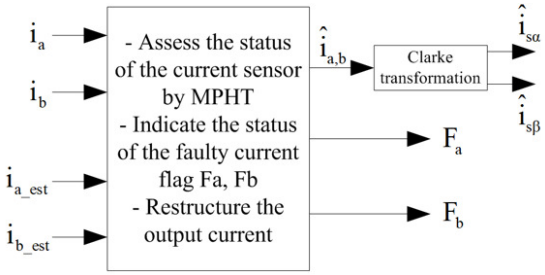

Fig. 4. The current sensor evaluation diagram.

In the proposed FTC architecture, the symbols $\hat{i}_a$ and $\hat{i}_b$ represent the reconstructed phase currents fed to the FOC algorithm when a sensor fault is detected. These reconstructed values are obtained from the estimated stator current components $\hat{i}_\alpha$ and $\hat{i}_\beta$, generated by LO in the stationary reference frame. Under normal operating conditions, $\hat{i}_a$ and $\hat{i}_b$ are equal to the measured phase currents from the sensors. Under fault conditions, the observer-based estimates $\hat{i}_\alpha$ and $\hat{i}_\beta$ are transformed through the inverse Clarke transform to provide accurate and reliable current signals to the FOC controller, ensuring continuous and stable motor operation.

V. SIMULATION RESULTS

To evaluate the effectiveness and reliability of the proposed FD method, a series of simulations were performed on an IM drive system operating under a FOC structure in the MATLAB/Simulink environment. These simulations included both soft current sensor and hard current sensor fault scenarios under no-load conditions. In addition, to investigate the sensor behavior under loaded conditions, two additional fault scenarios were simulated corresponding to scale and drift fault. These scenarios simulate real-world conditions when the IM operates under load condition, where sensor saturation and thermal drift are more likely to occur. In the test, the motor was driven at a reference speed from standstill to 750 rpm during the first 2.5 s of operation. All motor parameters used in the study are summarized in Table II.

TABLE II. PARAMETERS OF THE IM

Name	Unit	Rating value
Rated power	W	3360
Rated torque	Nm	14.8
Rated frequency	Hz	50
Nominal speed	rpm	1420
Pole pair number	-	2
Stator/rotor resistance	Ω	3.179/2.118
Stator/rotor inductance	H	0.209/0.209
Magnetizing inductance	H	0.192

A. *Fault Detection Performance for Soft Faults under No-Load Condition*

Soft faults were simulated to evaluate the robustness of the proposed FD and FTC framework. Four types of soft faults, drift, scale, bias, and precision degradation, were simulated corresponding to the A-phase current measurements at 1.25 s. In all cases, the MPHT, applied to the absolute residual signal, effectively detected the anomalies with minimal delay, and the measured current was seamlessly replaced by the estimated current from the LO, maintaining the continuity of the control process, as shown in Figures 5-9. The fault flag for phase A was triggered in every case, indicating the test's sensitivity to different fault characteristics (Figure 9(a)). The rotor speed remained smooth and closely followed the reference value in all cases, demonstrating that the FTC mechanism preserved the system's stability and performance (Figure 9(b)).

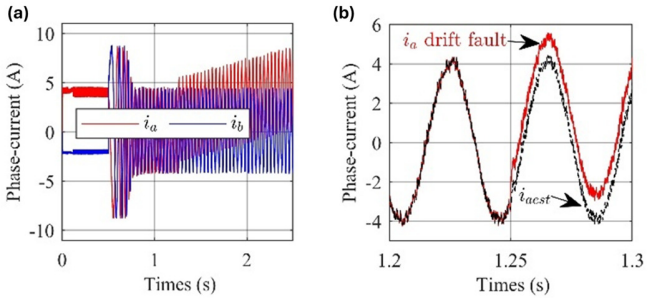

Fig. 5. Fault detection under drift fault in phase A: (a) measured phase currents and (b) comparison between faulty i_a and estimated current.

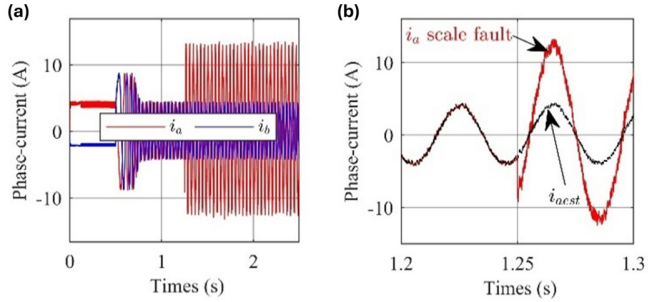

Fig. 6. Fault detection under scale fault in phase B: (a) measured phase currents and (b) comparison between faulty i_b and estimated current.

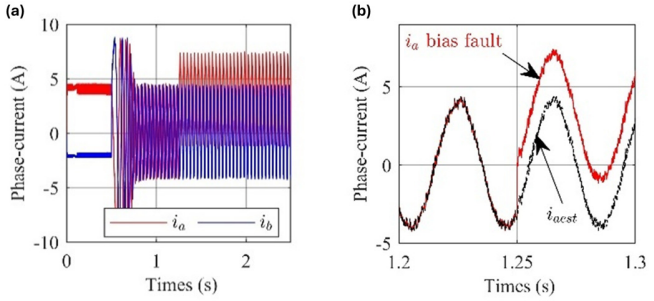

Fig. 7. Fault detection under bias fault in phase A: (a) measured phase currents and (b) comparison between faulty i_a and estimated current.

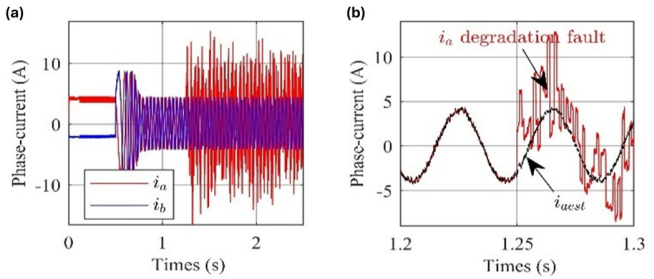

Fig. 8. Fault detection under precision degradation in phase A: (a) measured phase currents and (b) comparison between faulty i_a and estimated current.

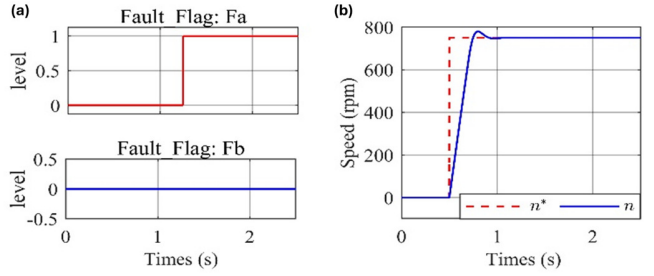

Fig. 9. System behavior under soft sensor faults: (a) fault detection flag for phases A and B and (b) rotor speed and reference.

B. Fault Detection Performance for Hard Faults under No-Load Condition

Three typical hard fault scenarios were simulated to validate the robustness of the proposed FD framework: a constant 3 A fault and a constant 3 A fault with noise. Each fault was simulated, corresponding to the B-phase current measurement at t = 1.25 s. The MPHT, applied to the absolute residual signal, effectively detected all fault conditions with minimal delay. Once detected, the FD mechanism triggered the LO to replace the corrupted current signal, ensuring continuity and stability during the control process. The results are depicted in Figures 10-13. Despite the sudden and severe nature of these faults, the fault flag for the B-phase was always triggered by the observer structure (Figure 13(a)), demonstrating accurate and continuous anomaly detection. Additionally, the rotor speed remains stable and closely follows the reference trajectory in all scenarios, confirming the effectiveness and resilience of the FTC strategy under hard fault conditions (Figure 13(b)).

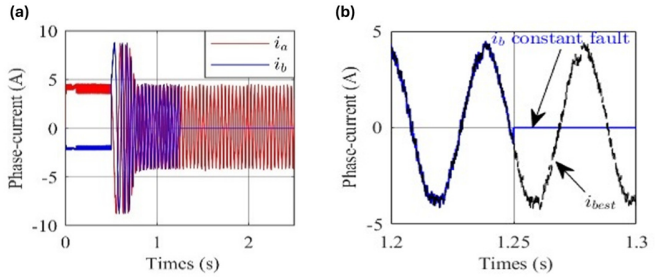

Fig. 10. Fault detection under constant-zero fault in phase A: (a) measured phase currents and (b) comparison between faulty $i_b = 0$ and estimated current.

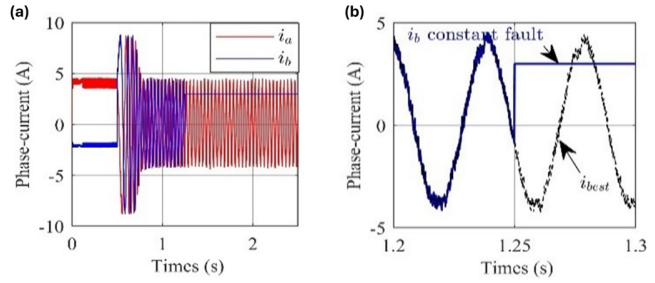

Fig. 11. Fault detection under constant-3A fault in phase B: (a) measured phase currents and (b) comparison between faulty i_b = 3A and estimated current.

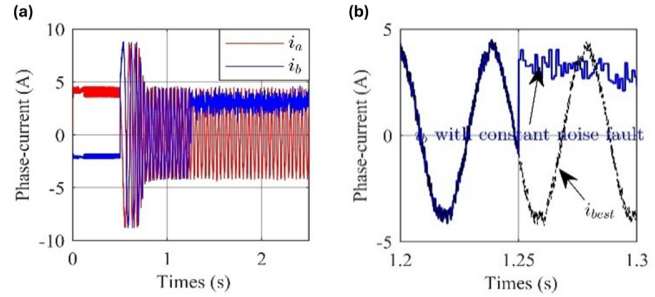

Fig. 12. Fault detection under constant-3A fault with noise in phase B: (a) measured phase currents and (b) comparison between noisy faulty i_b and estimated current.

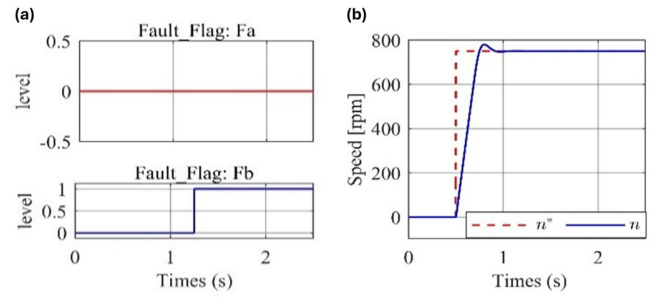

Fig. 13. System behavior under hard sensor faults: (a) fault detection flag for phases A and B and (b) rotor speed and reference.

C. Fault Detection Performance under 5 Nm Load Condition

To further validate the method under actual operating conditions, additional simulations were performed with the motor loaded at 5 Nm. Two typical soft faults, bias and drift, in the A-phase current sensor were examined. As illustrated in Figures 14-16, the FD mechanism maintained fast and accurate detection even under load, with the observer promptly compensating the error signals. Despite the load and gradual fault growth in the drift case, the proposed MPHT based detector maintained stable current regulation and accurate speed tracking, confirming the robustness of the method under real-world conditions.

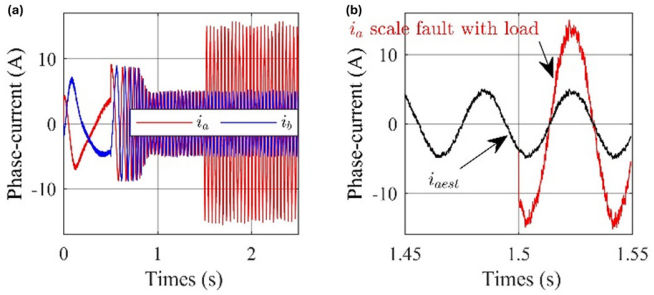

Fig. 14. Fault detection and current response under a phase-A bias fault at 5 Nm load: (a) measured phase currents and (b) comparison between faulty i_a and estimated current.

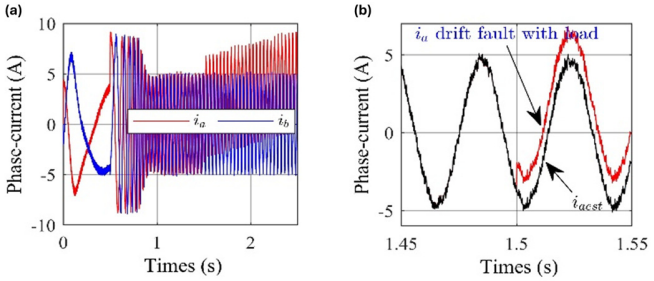

Fig. 15. Fault detection and current response under a phase-A drift fault at 5 Nm load: (a) measured phase currents, (b) comparison between faulty i_a and estimated current.

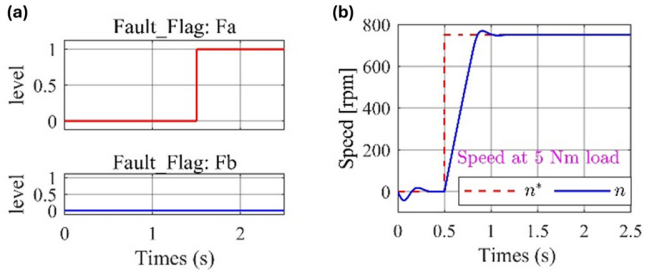

Fig. 16. System behavior under sensor faults with load at 5 Nm: (a) fault detection flag for phase A and (b) rotor speed and reference.

The simulation results in both soft and hard fault cases have confirmed the robustness, fast response, and reliability of the proposed fault detection method. Under all operating conditions, the MPHT-based detection algorithm accurately identifies sensor faults with minimal delay and quickly triggers the replacement of the fault measurement signal with the estimated value from the LO.

D. Quantitative Evaluation of Fault Detection Performance

To quantitatively evaluate the performance of the MPHT, the Δt , the ITSE, and the ITAE were compared, as defined in [16]:

$$\text{ITSE} = \frac{1}{n}\sum_{i=1}^{n}\int_{t=0}^{t=2} t.e^2(t)dt \quad (17)$$

$$\text{ITAE} = \frac{1}{n}\sum_{i=1}^{n}\int_{t=0}^{t=2} t.|e(t)|dt \quad (18)$$

where e(t) denotes the error between the measured and observer estimated current signals.

As outlined in Table III, the proposed MPHT algorithm demonstrates superior detection performance compared to the conventional ITAE and ITSE metrics described by (17) and (18). Specifically, the MPHT achieves fault detection within 0.1–0.6 ms, which is significantly faster than the traditional methods that require tens to hundreds of ms. This improvement is consistently demonstrated for both soft errors (drift, scale, skew, and precision degradation) and hard errors (constant and constant with noise) under both no-load and 5 Nm load conditions.

The significantly reduced Dt confirms the high sensitivity and fast response of MPHT when applied to the absolute residual signal generated by the LO. Furthermore, the smooth rotor speed and stable current profile observed in Figures 9, 13, and 16 verify that the FTC system remains robust and maintains accurate regulation even under severe fault conditions.

TABLE III. COMPARISON OF FAULT DETECTION TIMES UNDER DIFFERENT OPERATING CONDITIONS

Operating condition	**Fault type**	**Δt (ms)**		
		ITAE [16]	**ITSE** [16]	**MPHT (proposed)**
Soft Faults under no-load	Drift	196.2	247.6	0.6
	Scale	211.3	112.5	0.1
	Bias	124.7	50	0.2
	Precision Degradation	111.9	70	0.1
Hard Faults under no-load	Constant-zero	55.5	53	0.4
	Constant-3A	53.6	52	0.1
	Constant-3A with noise	53.4	51.7	0.1
Faults under load	Bias	106.5	50	0.2
	Drift	158.3	93.3	0.4

VI. CONCLUSIONS

This study proposed a comprehensive Fault-Tolerant Control (FTC) and diagnosis framework for induction motor drives, which combines the Luenberger Observer (LO) and the Modified Page–Hinkley Test (MPHT) algorithm. The simulation results demonstrate that the MPHT-based fault detector has significantly faster and more accurate detection capabilities than traditional indicators. In all tested scenarios,

the high sensitivity and real time performance of the proposed method were demonstrated. In addition, the FTC mechanism still maintains stable current and rotor speed regulation without requiring controller recalibrating, even under severe fault conditions. The obtained results confirm that the proposed method is a compact, efficient, and reliable solution for current sensor fault detection in field oriented control systems. Future research will focus on experimental validation and extending this framework to handle multi-sensor and parameter faults, thereby enhancing its reliability and applicability in real industrial settings.

ACKNOWLEDGMENT

This research was funded by the Student Grant Competition of VSB-Technical University of Ostrava under grant number SP2025/066 and by Ton Duc Thang University.

REFERENCES

[1] A. El-Shahat, *Induction Motors - Recent Advances, New Perspectives and Applications*, Rijeka, Croatia: IntechOpen, 2023.

[2] B. S. S. G. Yelamarthi and S. R. Sandepudi, "An Improved Fault Tolerant Converter Topology for Field Oriented Controlled Induction Motor Drive," *in 2019 International Conference on Power Electronics, Control and Automation (ICPECA)*, New Delhi, India, Nov. 2019, pp. 1–5, https://doi.org/10.1109/ICPECA47973.2019.8975694.

[3] D. H. Bach and C. D. Tran, "An improved voltage model based on stator resistance estimation for FOC technique in the induction motor drive," *Advances in Electrical and Electronic Engineering*, vol. 22, no. 2, pp. 107–114, June 2024, https://doi.org/10.15598/aeee.v22i2.5745.

[4] M. Aktas, K. Awaili, M. Ehsani, and A. Arisoy, "Direct torque control versus indirect field-oriented control of induction motors for electric vehicle applications," *Engineering Science and Technology, an International Journal*, vol. 23, no. 5, pp. 1134–1143, Oct. 2020, https://doi.org/10.1016/j.jestch.2020.04.002.

[5] E. Agamloh, A. von Jouanne, and A. Yokochi, "An Overview of Electric Machine Trends in Modern Electric Vehicles," *Machines*, vol. 8, no. 2, 2020, Art. no. 20, https://doi.org/10.3390/machines8020020.

[6] K. Rahman *et al*., "Field-Oriented Control of Five-Phase Induction Motor Fed From Space Vector Modulated Matrix Converter," *IEEE Access*, vol. 10, pp. 17996–18007, 2022, https://doi.org/10.1109/ACCESS.2022.3142014.

[7] M. Adamczyk, S. Niczyporuk, and T. Orlowska-Kowalska, "Current Sensor Fault-Tolerant Induction Motor Drive with Online Rotor Resistance Adaptation," *in 2022 IEEE 20th International Power Electronics and Motion Control Conference (PEMC)*, Brasov, Romania, Sept. 2022, pp. 546–552, https://doi.org/10.1109/PEMC51159.2022.9962895.

[8] M. S. Zaky and M. K. Metwaly, "Sensitivity Analysis of a Stator Current-based MRAS Estimator for Sensorless Induction Motor Drives," *Engineering, Technology & Applied Science Research*, vol. 14, no. 6, pp. 17584–17590, Dec. 2024, https://doi.org/10.48084/etasr.8737.

[9] Y. Chen, D. Xie, Y. Zuo, Y. Chang, and X. Ge, "Current Sensor Fault-Tolerant Control for Induction Motor with Speed-Sensorless Based on SMO and SEPLL," *in 2021 24th International Conference on Electrical Machines and Systems (ICEMS)*, Gyeongju, South Korea, Oct.-Nov. 2021, pp. 1988–1992, https://doi.org/10.23919/ICEMS52562.2021.9634408.

[10] M. Manohar and S. Das, "Current Sensor Fault-Tolerant Control for Direct Torque Control of Induction Motor Drive Using Flux-Linkage Observer," *IEEE Transactions on Industrial Informatics*, vol. 13, no. 6, pp. 2824–2833, Sept. 2017, https://doi.org/10.1109/TII.2017.2714675.

[11] Y. Azzoug *et al*., "An Active Fault-Tolerant Control Strategy for Current Sensors Failure for Induction Motor Drives Using a Single Observer for Currents Estimation and Axes Transformation," *European Journal of Electrical Engineering*, vol. 23, no. 6, pp. 467–474, Dec. 2021, https://doi.org/10.18280/ejee.230606.

[12] C. D. Tran, M. Kuchar, V. Sotola, and P. D. Nguyen, "Fault-Tolerant Control Based on Current Space Vectors against Total Sensor Failures," *Sensors*, vol. 24, no. 11, 2024, Art. no. 3558, https://doi.org/10.3390/s24113558.

[13] Y. Li and P. Gong, "Fault-tolerant control of induction motor with current sensors based on dual-torque model," *Energies*, vol. 16, no. 8, 2023, Art. no. 3442, https://doi.org/10.3390/en16083442.

[14] C. D. Tran, P. Palacky, M. Kuchar, P. Brandstetter, and B. H. Dinh, "Current and Speed Sensor Fault Diagnosis Method Applied to Induction Motor Drive," *IEEE Access*, vol. 9, pp. 38660–38672, 2021, https://doi.org/10.1109/ACCESS.2021.3064016.

[15] D. Diallo, M. E. H. Benbouzid, and A. Makouf, "A fault-tolerant control architecture for induction motor drives in automotive applications," *IEEE Transactions on Vehicular Technology*, vol. 53, no. 6, pp. 1847–1855, Nov. 2004, https://doi.org/10.1109/TVT.2004.833610.

[16] M. Dybkowski and K. Klimkowski, "Artificial neural network application for current sensors fault detection in the vector controlled induction motor drive," *Sensors*, vol. 19, no. 3, 2019, Art. no. 571, https://doi.org/10.3390/s19030571.

[17] E. H. El Bouchikhi, V. Choqueuse, and M. Benbouzid, "Induction machine faults detection using stator current parametric spectral estimation," *Mechanical Systems and Signal Processing*, vol. 52–53, pp. 447–464, Feb. 2015, https://doi.org/10.1016/j.ymssp.2014.06.015.

[18] T. Amanuel, A. Ghirmay, H. Ghebremeskel, R. Ghebrehiwet, and W. Bahlibi, "Comparative analysis of signal processing techniques for fault detection in three phase induction motor," *Journal of Electronics*, vol. 03, no. 01, pp. 61–76, 2021, https://doi.org/10.36548/jei.2021.1.006.

[19] H.-C. Chang, Y.-M. Jheng, C.-C. Kuo, and Y.-M. Hsueh, "Induction Motors Condition Monitoring System with Fault Diagnosis Using a Hybrid Approach," *Energies*, vol. 12, no. 8, 2019, Art. no. 1471, https://doi.org/10.3390/en12081471.

[20] S. Chikkam and S. Singh, "Condition Monitoring and Fault Diagnosis of Induction Motor using DWT and ANN," *Arabian Journal for Science and Engineering*, vol. 48, pp. 6237–6252, May 2023, https://doi.org/10.1007/s13369-022-07294-3.

[21] R. Sebastião and J. M. Fernandes, "Supporting the Page-Hinkley Test with Empirical Mode Decomposition for Change Detection," *Foundations of Intelligent Systems: 23rd International Symposium on Methodologies for Intelligent Systems (ISMIS)*, Warsaw, Poland, June 2017, pp. 492–498, https://doi.org/10.1007/978-3-319-60438-1_48.

[22] T. Andrianajaiana, T. D. Razafimahefa, D. A. Youssouf, R. N. Rakotoarijaona, E. J. R. Sambatra, and D. D. Lucache, "Fault Detection Device for PV Array using the Page-Hinkley Test," *in 2022 International Conference and Exposition on Electrical And Power Engineering (EPE)*, Iasi, Romania, Oct. 2022, pp. 505–510, https://doi.org/10.1109/EPE56121.2022.9959755.

[23] Y. Azzoug, R. Pusca, M. Sahraoui, A. Ammar, R. Romary, and A. J. Marques Cardoso, "A Single Observer for Currents Estimation in Sensor's Fault-Tolerant Control of Induction Motor Drives," *in 2019 International Conference on Applied Automation and Industrial Diagnostics (ICAAID)*, Elazig, Turkey, Sept. 2019, pp. 1–6, https://doi.org/10.1109/ICAAID.2019.8934969.

[24] Y. Azzoug, M. Sahraoui, R. Pusca, T. Ameid, R. Romary, and A. J. Marques Cardoso, "Current sensors fault detection and tolerant control strategy for three-phase induction motor drives," *Electrical Engineering*, vol. 103, pp. 881–898, Apr. 2021, https://doi.org/10.1007/s00202-020-01120-5.

[25] Y. Yu, Y. Zhao, B. Wang, X. Huang, and D. Xu, "Current Sensor Fault Diagnosis and Tolerant Control for VSI-Based Induction Motor Drives," *IEEE Transactions on Power Electronics*, vol. 33, no. 5, pp. 4238–4248, May 2018, https://doi.org/10.1109/TPEL.2017.2713482.

[26] C. Chakraborty and V. Verma, "Speed and Current Sensor Fault Detection and Isolation Technique for Induction Motor Drive Using Axes Transformation," *in IEEE Transactions on Industrial Electronics*, vol. 62, no. 3, pp. 1943–1954, Mar. 2015, https://doi.org/10.1109/TIE.2014.2345337.

AUTHORS PROFILE

Cuong Dinh Tran was born in Vietnam. He received his Ph.D. in Electrical Engineering from VSB-Technical University of Ostrava, Czech Republic, in 2020. Now, his current position is as a Deputy Head of the Electrical Engineering Department at the Faculty of Electrical and Electronics Engineering, Ton Duc Thang University, Ho Chi Minh City, Vietnam. His research interests focused on the application of modern control methods and intelligent algorithms in induction motor drives. He can be contacted at email: trandinhcuong@tdtu.edu.vn.

Martin Kuchar was born in Ostrava, Czech Republic. He received his MSc and PhD in Electrical Engineering from the Technical University of Ostrava (VSB) in 2000 and 2003, respectively. He has worked for many years as a Research and Development (R&D) Engineer and is currently an Associate Professor at the Department of Electronics, Faculty of Electrical Engineering and Computer Science, VSB-Technical University of Ostrava. His research focuses on DSC-based control, sensorless and fault-tolerant control of AC drives. He can be reached at martin.kuchar@vsb.cz.

Phuong Duy Nguyen is a lecturer at the Faculty of Engineering and Technology, Saigon University. He received his B.E. from Ho Chi Minh City University of Technology and Education (2010) and M.E. from Ho Chi Minh City University of Technology (2014). He is currently a PhD student at the Faculty of Electrical Engineering & Computer Science, VSB-Technical University of Ostrava, Czech Republic. His research interests include modern control methods, intelligent algorithms for motor drives, and power systems. Contact email: phuong.nd@sgu.edu.vn; phuong.nguyen.duy.st@vsb.cz.